Strain Induced by Evaporated-Metal Contacts on Monolayer MoS_2 Transistors

Marc Jaikissoon, *Graduate Student Member, IEEE*, Eric Pop, *Fellow, IEEE*, and Krishna C. Saraswat, *Life Fellow, IEEE*

***Abstract*— Electron-beam evaporation is commonly used to form metal contacts on two-dimensional (2D) materials. Many evaporated metals contain high levels of stress, but the effect of this stress on 2D device performance has yet to be determined. Here, we investigate the impact of tensile-stressed nickel evaporated onto gold contacts of monolayer MoS_2 transistors. Optical measurements reveal a distribution of tensile strain along the MoS_2 channel between stressed contacts, up to ∼0.8% near the contact edges. Further, we show that stressed contacts can substantially influence device performance, leading to negative threshold voltage shifts and increased transconductance. In the limit of short (50 nm) channels with large (2 μm) contact stressors, we find that this can cause an on-state current increase up to 2.5x. These results show that contact-induced strain must be closely examined in emerging technologies, and this approach could be used to improve future device performance.**

***Index Terms*— MoS_2, monolayer, tensile stress, strain, e-beam evaporation, contacts.**

I. Introduction

TRANSITION metal dichalcogenides (TMDs) such as monolayer (1L) molybdenum disulfide (MoS_2) are a class of two-dimensional (2D) semiconductors which show great promise for transistor applications owing to their ultra-thin body, offering increased robustness to short-channel effects [1], [2]. Recently, there have been several advances in contact engineering for monolayer MoS_2, including through the use of doping [3] or novel contact metals [4], [5] and alloys [6]. Electron-beam evaporation (EBE) remains the most commonly used technique for metal contact formation due to its ease of use, lift-off compatibility and the availability of a wide range of materials.

Manuscript received 21 May 2024; accepted 24 May 2024. Date of publication 5 June 2024; date of current version 26 July 2024. This work was supported in part by Stanford Nanofabrication Facility (SNF) and Stanford Nano Shared Facilities (SNSF) funded by the National Science Foundation (NSF) under Award ECCS-2026822; and in part by Stanford SystemX Alliance, Samsung Global Research Outreach (GRO) Program, and Intel Corp. The work of Marc Jaikissoon was supported by a Stanford Graduate Fellowship. The work of Eric Pop was supported by the SUPREME JUMP 2.0 Center, a Semiconductor Research Corporation (SRC) Program sponsored by Defense Advanced Research Projects Agency (DARPA). The review of this letter was arranged by Editor A. E. Islam. *(Corresponding author: Krishna C. Saraswat.)*

The authors are with the Department of Electrical Engineering, Stanford University, Stanford, CA 94305 USA (e-mail: saraswat@stanford.edu).

Digital Object Identifier 10.1109/LED.2024.3410095

It is known that EBE of several common metals, such as Ni and Pt, results in thin films which can contain high levels of residual stress [7], [8]. This can often be deleterious for conventional Si devices [9], but has been previously leveraged to induce strain in graphene and $MoTe_2$ through the evaporation of Ni with controlled amounts of tensile stress [10], [11]. However, metal-induced strain and its effect on TMD transistor behavior has not been studied before. Given that many recent advances in contact engineering utilize metals with unknown amounts of stress, it is crucial to understand the role that stress in the contact region can play in device performance.

Here, we report the first study of contact-metal-induced strain in monolayer MoS_2 transistors, using Au contacts capped by tensile-stressed EBE-Ni. By Raman spectroscopy, we probe the distribution of strain along the channel before and after Ni deposition, observing peak strains up to 0.8% near the contacts. Electrical measurements reveal negative threshold shifts and improved transconductance with increasing Ni stressor thickness. We also find the strain effect can be influenced by the contact size, resulting in large changes of transistor performance especially for short (50 nm) channels.

II. Fabrication and Measurement

Fig. 1(a) shows the cross-sectional schematic of our devices fabricated with strained contacts. We grow monolayer MoS_2 by chemical vapor deposition at 750 °C onto 90 nm SiO_2 on p^{++} Si substrates, which also serve as back-gates [12]. All patterning steps are done by electron-beam lithography (EBL). Channel regions are defined by XeF_2 etching, transistors receive probe pads (2 nm Ti/20 nm Pt), optical test structures do not. All devices have Au (50 nm) contacts, deposited by EBE at $\sim 10^{-8}$ Torr and 0.5 Å/s [13]. For transistors, the same Au step is used to connect the contacts to the probe pads. At this point, we take optical and electrical measurements to obtain a reference value for devices before the Ni stressors are added. Then, we use EBL to define overlaid regions above each Au contact, filled with 2 nm Ti/50 nm Ni by EBE at $\sim 10^{-6}$ Torr and 1.5 Å/s. A top-down scanning electron microscope image of a device is in Fig. 1(b).

We evaluated the stress of EBE-Ni on reference 100 mm Si wafers by radius of curvature measurements [14], finding these deposition conditions yield films with ∼800 MPa tensile stress. Lowering the deposition rate or pressure was found to reduce this stress, in accordance with literature [7].

0741-3106 © 2024 IEEE. Personal use is permitted, but republication/redistribution requires IEEE permission.
See https://www.ieee.org/publications/rights/index.html for more information.

Authorized licensed use limited to: Stanford University. Downloaded on July 28,2024 at 00:28:48 UTC from IEEE Xplore. Restrictions apply.

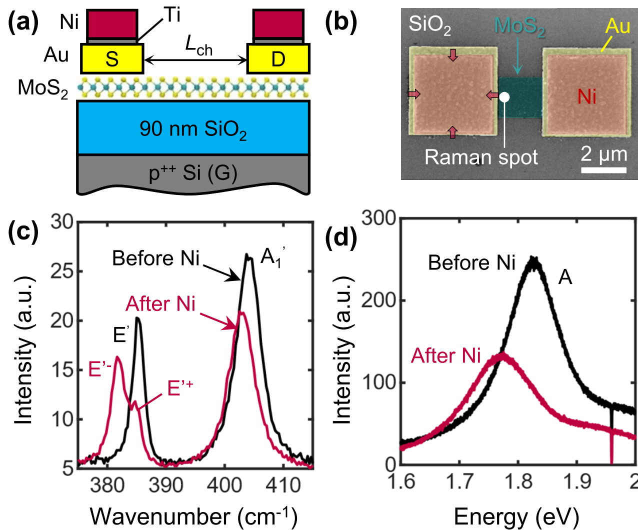

Fig. 1. **(a)** Cross-sectional schematic of monolayer MoS_2 device with Au contacts, each capped by a tensile Ni stressor layer (~800 MPa). S, D, and G mark the source, drain, and gate. **(b)** Top-down, colorized scanning electron microscope image of the device in **(a)**. Red arrows indicate the relaxation of tensile-stressed Ni. **(c)** Raman and **(d)** photoluminescence (PL) spectra of monolayer MoS_2 near the contact edge, as marked in **(b)**, before and after Ni capping.

Optical measurements were performed with a 532 nm laser, ~0.5 μm spot size, and 2.5% nominal laser power of the Horiba LabRam instrument (corresponding to incident power of 0.56 mW and a temperature rise < 10 K of the MoS_2 [15]). Electrical measurements were taken in ~10^{-5} Torr vacuum after a pre-measurement anneal at 250 °C for 2 hours.

III. Results and Discussion

A. Optical Measurements

Raman spectra of the MoS_2 channel near a contact before and after Ni capping are shown in Fig. 1(c). We note a red-shift of the E' peak after Ni capping, and splitting into the E'^{+} and E'^{-} peaks, known to appear at high tensile strain [16]. The E'^{-} position of 381.9 cm^{-1} and E'^{+} of 384.8 cm^{-1} correspond to ~0.8% uniaxial tensile strain in MoS_2 near the contact edge. The photoluminescence (PL) spectrum shown in Fig. 1(d) displays an A exciton red-shift of ~55 meV after capping, consistent with the strain indicated by Raman. Tensile strain lowers the K-point conduction band and raises the Γ-point valence band [16], [17] of MoS_2, narrowing both the direct gap (A exciton red-shift) and the indirect gap (lower PL intensity), while increasing the Q-K valley separation in the conduction band [18].

To probe the strain distribution along a 2 μm MoS_2 channel, we take a sequence of Raman spectra as illustrated in Fig. 2(a), in steps of 0.5 μm. Fig. 2(b) shows five spectra acquired along the channel direction, before and after Ni stressor deposition. Near the contact edges, E' red-shift and peak splitting is visible after Ni capping, whereas a smaller red-shift is observed near the channel center. This indicates a tensile strain profile that is highest near the contacts, decaying toward the center of the channel. The Ni capping the Au contacts contracts to relieve its own stress, thereby 'pulling' on the MoS_2 beneath and transferring strain to the channel between the contacts. Fig. 2(c) summarizes the evolution of

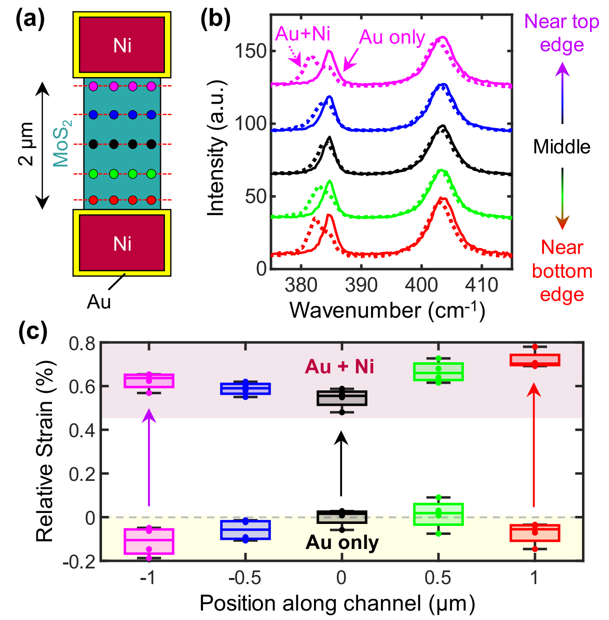

Fig. 2. **(a)** Top-down schematic of 2 μm MoS_2 channel showing where Raman spectra are acquired (circles). **(b)** Variation of Raman spectra from near the top contact (magenta) to near the bottom contact (red). **(c)** Estimated strain at each position along the MoS_2 channel, before and after Ni deposition, from near the top (magenta) to near the bottom contact (red). Each box averages the four spectra (four symbols per box) taken across the channel width, corresponding to the symbols on horizontal lines in **(a)**.

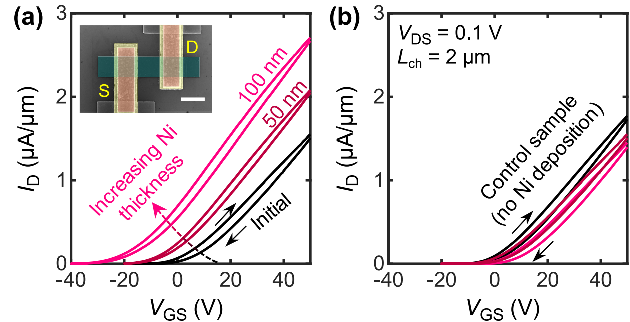

Fig. 3. Measured transfer characteristics of **(a)** back-gated monolayer MoS_2 transistor with increasing thickness of Ni stressor at the contacts, and **(b)** control device on the same chip which experienced the same thermal budget without any Ni deposition. Inset shows top-down colorized scanning electron microscope image of a device; scale bar is 2 μm. Small arrows mark forward and backward sweeps [22].

the estimated strain along the channel, relative to the E' peak (385.1 cm^{-1}) at the device center before Ni deposition. Prior to Ni deposition we also note small relative compressive strain near the Au contacts [19], but significant tensile strain appears along the channel after Ni-capping the contacts. (We do not expect charge transfer doping from the Ni stressor layer, because the Au contacts are 50 nm thick.)

B. Electrical Measurements

We next investigate the effect of contact-induced strain on transistor performance. Fig. 3(a) shows measured I_D vs. V_{GS} of a back-gated transistor with channel length $L_{ch} = 2$ μm measured after different thicknesses of Ni capping. We observe that, compared to the initial case of pure Au contacts, capping the contacts with 50 nm Ni stressor causes a negative threshold voltage shift ($\Delta V_T \approx -10$ V), as well as a 10% increase in

Authorized licensed use limited to: Stanford University. Downloaded on July 28,2024 at 00:28:48 UTC from IEEE Xplore. Restrictions apply.

the device transconductance ($= \partial I_D/\partial V_{GS}$). This results in an overall increase of the maximum device current, which is consistent with recent measurements of tensile strain in MoS_2 [17], [20], [21]. By increasing the Ni stressor thickness to 100 nm, the threshold voltage V_T and transconductance continue the same trend. In comparison, Fig. 3(b) shows measured I_D vs. V_{GS} of a control device on the same chip, which experienced the same thermal budget but without Ni deposition onto the Au contacts. This control device indicates very little change in behavior, confirming a Ni-strain-induced origin of the changes observed in Fig. 3(a).

We note that the pre-measurement anneal which all devices receive (250 °C for 2 hours, in vacuum), and any additional thermal processing during fabrication, may affect the stress in the contact metal stack and is a topic which warrants further investigation. For example, Au thin films can experience increased tensile stress after annealing, due to changes in the grain structure [23], [24]. This does not affect the conclusions of the present work, although it may contribute an additional source of tensile strain in the channel of both control and experimental devices, which receive the same anneal. Understanding other sources of process-induced strain, including various annealing steps, is a topic for future work and will be crucial to the eventual implementation of strain in TMD transistors.

Finally, we turn our attention to the effect of strained-contact size on transistor behavior. Because the dimensions of the stressor layer are known to influence the induced strain in the TMD [25], we fabricate devices with fixed channel lengths (L_{ch} = 2 μm, 100 nm and 50 nm) and variable contact lengths (L_c = 2 μm, 1 μm, 500 nm and 200 nm) as shown in Fig. 4(a-d) for L_{ch} = 50 nm. The channel width, W, is fixed at 1 μm for all devices, allowing us to study the effect of strain in devices with aspect ratios ($AR = W/L_{ch}$) increasing from 0.5 to 20. The values of L_c are chosen to remain well above typical contact transfer lengths (10-100 nm with Au contacts on MoS_2) to avoid size-dependent contact resistance (R_c) [13], [26], [27]. We note that for these devices, Au/Ti/Ni deposition is done in one combined step with 40 nm Ni stressor thickness.

Fig. 4(e) shows the measured I_D vs. V_{GS} for the shortest-channel devices (L_{ch} = 50 nm) with the four contact lengths (L_c = 0.2 μm, 0.5 μm, 1 μm, 2 μm). With increasing L_c, we observe negative V_T shifting and substantial increases in peak transconductance, causing up to 2.5× change of peak current, depending on the size of the stressor.

To account for V_T shifting, Fig. 4(f) shows box plots of on-state current, I_{on}, extracted at a fixed carrier density $n \approx 10^{13}$ cm^{-2} [22] to capture the effect of increasing L_c (with Ni stressor) on transistor performance. For long channels (top panel, L_{ch} = 2 μm), changing the stressor size only has a minor impact on device performance, increasing I_{on} by just a few percent. However, for 100 nm channel length (middle panel), we observe that stressor sizes of $L_c > 0.5$ μm begin to increase I_{on}, up to 2× in the case of L_c = 2 μm. The effect is most significant for L_{ch} = 50 nm (bottom panel), where we see I_{on} increasing by up to 3× as L_c increases from 0.2 to 2 μm. In other words, devices with larger W/L_{ch} aspect ratios experience greater improvements under strain. We note

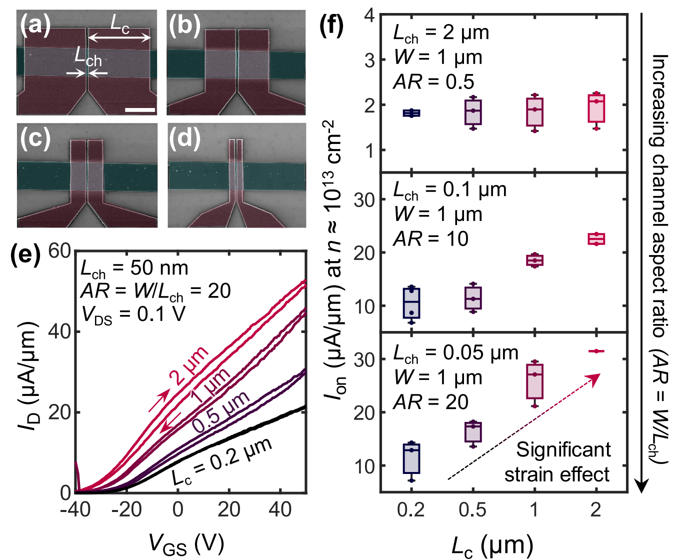

Fig. 4. Colorized scanning electron microscope image of back-gated monolayer MoS_2 transistors with channel length L_{ch} = 50 nm and contact length (a) L_c = 2 μm, (b) L_c = 1 μm, (c) L_c = 0.5 μm, and (d) L_c = 0.2 μm. Inset scale bar is 1 μm. All devices received 40 nm Ni stressor layer on top of their Au contacts. (e) Measured transfer characteristics of devices shown in (a)-(d). Small arrows mark forward and backward V_{GS} sweeps [22]. (f) Box plots summarizing on-state current (I_{on}) at fixed carrier density $n \approx 10^{13}$ cm^{-2} and V_{DS} = 0.1 V for devices with channel lengths L_{ch} = 2 μm, 0.1 μm and 0.05 μm (corresponding to aspect ratios $AR = W/L_{ch}$ = 0.5, 10 and 20, respectively) and varying contact lengths, L_c. The L_c plays by far the strongest role in the shortest-channel devices, due to the contact-induced strain.

that the device yield decreases for short channels with long contacts, as the MoS_2 channel frequently begins to tear, which is reflective of the high strains sustained in this regime.

These results indicate that short channel devices benefit the most from contact-induced tensile strain in the MoS_2 channel. Given the strain profile observed in Fig. 2, we believe that one potential source of this improvement is the presence of a larger average tensile strain retained in shorter channels compared to longer channels, where the strain can decay toward the channel center. Additionally, the increasing contribution of R_c to the overall resistance of short channel devices hints that contact-induced strain may act to reduce R_c [21], [28]. As such, it is crucial for future contact metal investigations to include strain analysis as a potential source of improvement.

IV. Conclusion

In conclusion, we report the first observation of contact-metal induced tensile strain in monolayer MoS_2 transistors using Ni stressor layers on the contact regions. We observe a tensile strain gradient between the source and drain contacts, up to 0.8% near the edges. Further, we show that this strain can act to increase on-state current, especially for shorter-channel devices (here, ∼50 nm). This makes contact-induced strain a viable technique to engineer contact resistance, and therefore we recommend that future studies related to contact improvements to TMDs incorporate strain into the device analysis.

Acknowledgment

The authors acknowledge Dante Zakhidov and Lauren Hoang for help with Raman measurements.

Authorized licensed use limited to: Stanford University. Downloaded on July 28,2024 at 00:28:48 UTC from IEEE Xplore. Restrictions apply.

REFERENCES

[1] C. Gilardi, R. K. A. Bennett, Y. Yoon, E. Pop, H.-S. P. Wong, and S. Mitra, "Extended scale length theory for low-dimensional field-effect transistors," *IEEE Trans. Electron Devices*, vol. 69, no. 9, pp. 5302–5309, Sep. 2022, doi: 10.1109/TED.2022.3190464.

[2] S. Das, A. Sebastian, E. Pop, C. J. McClellan, A. D. Franklin, T. Grasser, T. Knobloch, Y. Illarionov, A. V. Penumatcha, J. Appenzeller, Z. Chen, W. Zhu, I. Asselberghs, L.-J. Li, U. E. Avci, N. Bhat, T. D. Anthopoulos, and R. Singh, "Transistors based on two-dimensional materials for future integrated circuits," *Nature Electron.*, vol. 4, no. 11, pp. 786–799, Nov. 2021, doi: 10.1038/s41928-021-00670-1.

[3] C. J. McClellan, E. Yalon, K. K. H. Smithe, S. V. Suryavanshi, and E. Pop, "High current density in monolayer MoS_2 doped by AlO_x," *ACS Nano*, vol. 15, no. 1, pp. 1587–1596, Jan. 2021, doi: 10.1021/acsnano.0c09078.

[4] W. Li, X. Gong, Z. Yu, L. Ma, W. Sun, S. Gao, Ç. Köroğlu, W. Wang, L. Liu, T. Li, H. Ning, D. Fan, Y. Xu, X. Tu, T. Xu, L. Sun, W. Wang, J. Lu, Z. Ni, J. Li, X. Duan, P. Wang, Y. Nie, H. Qiu, Y. Shi, E. Pop, J. Wang, and X. Wang, "Approaching the quantum limit in two-dimensional semiconductor contacts," *Nature*, vol. 613, no. 7943, pp. 274–279, Jan. 2023, doi: 10.1038/s41586-022-05431-4.

[5] P.-C. Shen, C. Su, Y. Lin, A.-S. Chou, C.-C. Cheng, J.-H. Park, M.-H. Chiu, A.-Y. Lu, H.-L. Tang, M. M. Tavakoli, G. Pitner, X. Ji, Z. Cai, N. Mao, J. Wang, V. Tung, J. Li, J. Bokor, A. Zettl, C.-I. Wu, T. Palacios, L.-J. Li, and J. Kong, "Ultralow contact resistance between semimetal and monolayer semiconductors," *Nature*, vol. 593, no. 7858, pp. 211–217, May 2021, doi: 10.1038/s41586-021-03472-9.

[6] A. Kumar, K. Schauble, K. M. Neilson, A. Tang, P. Ramesh, H.-S. P. Wong, E. Pop, and K. Saraswat, "Sub-200 $\Omega\cdot\mu$m alloyed contacts to synthetic monolayer MoS_2," in *IEDM Tech. Dig.*, Dec. 2021, pp. 7.3.1–7.3.4, doi: 10.1109/IEDM19574.2021.9720609.

[7] H. Z. Yu and C. V. Thompson, "Grain growth and complex stress evolution during Volmer–Weber growth of polycrystalline thin films," *Acta Mater.*, vol. 67, pp. 189–198, Apr. 2014, doi: 10.1016/j.actamat.2013.12.031.

[8] E. Klokholm and B. S. Berry, "Intrinsic stress in evaporated metal films," *J. Electrochem. Soc.*, vol. 115, no. 8, p. 823, 1968, doi: 10.1149/1.2411441.

[9] T. Guillaume, M. Mouis, S. Maitrejean, A. Poncet, M. Vinet, and S. Deleonibus, "Evaluation of strain-induced mobility variation in TiN metal gate SOI n-MOSFETs," in *Proc. 30th Eur. Solid-State Circuits Conf.*, Mar. 2004, pp. 393–396, doi: 10.1109/ESSDER.2004.1356572.

[10] H. Shioya, S. Russo, M. Yamamoto, M. F. Craciun, and S. Tarucha, "Electron states of uniaxially strained graphene," *Nano Lett.*, vol. 15, no. 12, pp. 7943–7948, Dec. 2015, doi: 10.1021/acs.nanolett.5b03027.

[11] W. Hou, A. Azizimanesh, A. Sewaket, T. Peña, C. Watson, M. Liu, H. Askari, and S. M. Wu, "Strain-based room-temperature non-volatile $MoTe_2$ ferroelectric phase change transistor," *Nature Nanotechnol.*, vol. 14, no. 7, pp. 668–673, Jul. 2019, doi: 10.1038/s41565-019-0466-2.

[12] K. K. H. Smithe, C. D. English, S. V. Suryavanshi, and E. Pop, "Intrinsic electrical transport and performance projections of synthetic monolayer MoS_2 devices," *2D Mater.*, vol. 4, no. 1, Nov. 2017, Art. no. 011009, doi: 10.1088/2053-1583/4/1/011009.

[13] C. D. English, G. Shine, V. E. Dorgan, K. C. Saraswat, and E. Pop, "Improved contacts to MoS_2 transistors by ultra-high vacuum metal deposition," *Nano Lett.*, vol. 16, no. 6, pp. 3824–3830, Jun. 2016, doi: 10.1021/acs.nanolett.6b01309.

[14] G. G. Stoney, "The tension of metallic films deposited by electrolysis," *Proc. Roy. Soc. London A*, vol. 82, no. 553, pp. 172–175, May 1909, doi: 10.1098/rspa.1909.0021.

[15] E. Yalon, B. Aslan, K. K. H. Smithe, C. J. McClellan, S. V. Suryavanshi, F. Xiong, A. Sood, C. M. Neumann, X. Xu, K. E. Goodson, T. F. Heinz, and E. Pop, "Temperature-dependent thermal boundary conductance of monolayer MoS_2 by Raman thermometry," *ACS Appl. Mater. Interface*, vol. 9, no. 49, pp. 43013–43020, Dec. 2017, doi: 10.1021/acsami.7b11641.

[16] H. J. Conley, B. Wang, J. I. Ziegler, R. F. Haglund, S. T. Pantelides, and K. I. Bolotin, "Bandgap engineering of strained monolayer and bilayer MoS_2," *Nano Lett.*, vol. 13, no. 8, pp. 3626–3630, Aug. 2013, doi: 10.1021/nl4014748.

[17] I. M. Datye, A. Daus, R. W. Grady, K. Brenner, S. Vaziri, and E. Pop, "Strain-enhanced mobility of monolayer MoS_2," *Nano Lett.*, vol. 22, no. 20, pp. 8052–8059, Oct. 2022, doi: 10.1021/acs.nanolett.2c01707.

[18] M. Hosseini, M. Elahi, M. Pourfath, and D. Esseni, "Strain induced mobility modulation in single-layer MoS_2," *J. Phys. D, Appl. Phys.*, vol. 48, no. 37, Sep. 2015, Art. no. 375104, doi: 10.1088/0022-3727/48/37/375104.

[19] R. Abermann and R. Koch, "The internal stress in thin silver, copper and gold films," *Thin Solid Films*, vol. 129, nos. 1–2, pp. 71–78, Jul. 1985, doi: 10.1016/0040-6090(85)90096-3.

[20] Y. Zhang, H. L. Zhao, S. Huang, M. A. Hossain, and A. M. van der Zande, "Enhancing carrier mobility in monolayer MoS_2 transistors with process-induced strain," *ACS Nano*, vol. 18, no. 19, pp. 12377–12385, May 2024, doi: 10.1021/acsnano.4c01457.

[21] M. Jaikissoon, Ç. Köroğlu, J. A. Yang, K. M. Neilson, K. C. Saraswat, and E. Pop, "CMOS-compatible strain engineering for high-performance monolayer semiconductor transistors," 2024, *arXiv:2405.09792*.

[22] Z. Cheng, C.-S. Pang, P. Wang, S. T. Le, Y. Wu, D. Shahrjerdi, I. Radu, M. C. Lemme, L.-M. Peng, X. Duan, Z. Chen, J. Appenzeller, S. J. Koester, E. Pop, A. D. Franklin, and C. A. Richter, "How to report and benchmark emerging field-effect transistors," *Nature Electron.*, vol. 5, no. 7, pp. 416–423, Jul. 2022, doi: 10.1038/s41928-022-00798-8.

[23] S. Zhou, W. Wu, and T. Shao, "Effect of post deposition annealing on residual stress stability of gold films," *Surf. Coat. Technol.*, vol. 304, pp. 222–227, Oct. 2016, doi: 10.1016/j.surfcoat.2016.07.001.

[24] A. Prószyński, D. Chocyk, and G. Gładyszewski, "Stress modification in gold metal thin films during thermal annealing," *Optica Applicata*, vol. 39, pp. 705–710, Dec. 2009.

[25] A. Azizimanesh, T. Peña, A. Sewaket, W. Hou, and S. M. Wu, "Uniaxial and biaxial strain engineering in 2D MoS_2 with lithographically patterned thin film stressors," *Appl. Phys. Lett.*, vol. 118, no. 21, May 2021, Art. no. 213104, doi: 10.1063/5.0049446.

[26] T. F. Schranghamer, N. U. Sakib, M. U. K. Sadaf, S. Subbulakshmi Radhakrishnan, R. Pendurthi, A. D. Agyapong, S. P. Stepanoff, R. Torsi, C. Chen, J. M. Redwing, J. A. Robinson, D. E. Wolfe, S. E. Mohney, and S. Das, "Ultrascaled contacts to monolayer MoS_2 field effect transistors," *Nano Lett.*, vol. 23, no. 8, pp. 3426–3434, Apr. 2023, doi: 10.1021/acs.nanolett.3c00466.

[27] Q. Smets, G. Arutchelvan, J. Jussot, D. Verreck, I. Asselberghs, A. N. Mehta, A. Gaur, D. Lin, S. E. Kazzi, B. Groven, M. Caymax, and I. Radu, "Ultra-scaled MOCVD MoS_2 MOSFETs with 42 nm contact pitch and 250μA/μm drain current," in *IEDM Tech. Dig.*, Dec. 2019, pp. 23.2.1–23.2.4, doi: 10.1109/IEDM19573.2019.8993650.

[28] A. P. John, A. Thenapparambil, and M. Thalakulam, "Strain-engineering the Schottky barrier and electrical transport on MoS_2," *Nanotechnology*, vol. 31, no. 27, Apr. 2020, Art. no. 275703, doi: 10.1088/1361-6528/ab83b7.

Authorized licensed use limited to: Stanford University. Downloaded on July 28,2024 at 00:28:48 UTC from IEEE Xplore. Restrictions apply.